On the use of semiclassical dynamics in determining electronic spectra of Br_2 in an Ar matrix[a)]

D. Thirumalai,[b)] E. J. Bruskin, and B. J. Berne
Department of Chemistry, Columbia University, New York, New York 10027

(Received 4 March 1985; accepted 25 March 1985)

A semiclassical method to simulate the electronic absorption and emission spectra of Br_2 in an Ar matrix is presented. The appropriate time correlation functions are evaluated in the Condon approximation using Gaussian wave packet dynamics. Several approximate methods are used to propagate the wave packet and their relative merits in obtaining high resolution spectra are discussed. The dynamics using a single Gaussian wave packet is inadequate for obtaining spectra in highly anharmonic systems, frequently encountered in condensed phase problems. Where possible, the results of the simulation are compared in detail with available experiments. The simulated electronic absorption spectra confirm the physical picture advanced by Bondebey and Brus. It is shown that from the spectral analysis of the emission spectra one can infer some features of the guest–host interaction when the guest is in the electronically excited state.

I. INTRODUCTION

In recent years there have been several experimental studies of electronic spectra of halogen molecules in rare gas matrices (Ne, Ar, Kr, Xe) at low temperatures.[1–7] The study of small molecule electronic spectra in low temperature hosts can provide valuable information about the guest–host interaction, and radiationless transitions. Often this can lead to understanding of relaxation mechanisms in other systems as well. For example, it has been suggested that relaxation in a large molecule is similar to that of small molecules in low temperature hosts.[8] It is, therefore, of interest to simulate the electronic spectra of matrix isolated diatomics. In a system consisting of one Br_2 molecule dissolved in a rare gas matrix (Ar), we assume that all the degrees of freedom except the vibrational coordinate of Br_2 may be treated classically. This is justified because the low frequency Ar–Ar and Ar–Br vibrations can be approximated by classical mechanics, whereas the high frequency Br_2 vibration must be treated quantum mechanically. Because the moment of inertia of Br_2 is high, the rotational degrees of freedom of Br_2 are also treated classically. Herman and Berne[9,10] studied this system at higher temperatures and under conditions where the host was static. Here we study the dynamic effects of the matrix on the photochemistry of Br_2. For the purpose of obtaining the appropriate time correlation functions and consequently the electronic spectra we use the Gaussian wave packet dynamics developed by Heller[11–13] (suitably modified to treat mixed quantum-classical system considered here). The formalism described here is a semiclassical treatment of a quantum degree of freedom embedded in a classical solvent.

The purpose of this article is twofold: (a) Can we explain some features of the experimental spectra of diatoms in rare gas matices and obtain information regarding the nature of the guest–host interaction? (b) We want to assess the applicability of the Gaussian wave packet method for many-body problems of the sort considered here. We find that Gaussian wave packet dynamics gives low to medium resolution spectra. The reason for this is that the width of the wave packet increases abnormally as it explores the anharmonic wings of the potential surface, a problem exacerbated by the presence of the Ar matrix. Therefore, the propagation is only accurate over a short time interval with a concommitant decrease in frequency resolution. We believe the single Gaussian wave packet dynamics is simply not adequate to give high resolution spectrum. Unfortunately, the solvent–solute interaction potentials are not known so that comparison between the present simulation and experiment is to be taken as suggestive. Nevertheless, the algorithm described here is useful in predicting certain qualitative features and may be more suited for treating other dynamical phenomena in low temperature condensed phase systems (chemical reactions, photodissociation, etc.).

II. THEORY

Using linear response theory and electronic absorption line shape $I(\omega)$ can be expressed as[14]

$$I(\omega)=\frac{1}{2\pi}\int_{-\infty}^{\infty} dt\, e^{-i\omega t}\, C(t), \tag{1}$$

where $C(t)$ is the dipolar autocorrelation function which in the Born–Oppenheimer approximation for the transition from the electronic states i to f is given by

$$C(t)=\mathrm{Tr}\{\rho_i \mu_{if} e^{-iH_f t/\hbar}\mu_{if} e^{iH_i t/\hbar}\}/\mathrm{Tr}\{e^{-\beta H_i}\}. \tag{2}$$

In Eq. (2) ρ_i is the density operator $e^{-\beta H_i}$, μ_{if} is the electronic transition moment as a function of nuclear coordinates, H_i and H_f are the Hamiltonians for the system corresponding to the lower and upper potential surfaces, respectively, and $\beta = 1/kT$. The system consists of one quantum degree of freedom (corresponding to the vibrational coordinate of the Br_2 molecule) and f classical degrees of freedom, $\mathbf{X} = (X_1, X_2 \ldots X_f)$. The Hamiltonian of the system on the two surfaces $H_{i(f)}$ can be written as

a) Supported by the grant from NSF.

b) Present address: Department of Chemistry and the Institute for Physical Sciences and Technology, University of Maryland, College Park, MD 20742.

 0021-9606/85/130230-09$02.10

$$H_{i(f)} = T_Q + V_{i(f)}(Q) + V(Q,\mathbf{X}) + H(\mathbf{P},\mathbf{X}) \quad (3)$$

$$\equiv h_{i(f)}(Q,\mathbf{X}) + H(\mathbf{P},\mathbf{X}), \quad (4)$$

where T_Q is the kinetic energy operator for the relative motion of Br_2, $V_{i(f)}(Q)$ is the electronic potential surface for the lower (i) [upper (f)] electronic surfaces, $V(Q,\mathbf{X})$ is the potential of interaction between Q and $\mathbf{X}$ which for simplicity we take to be the same for states i and f, and $H(\mathbf{P},\mathbf{X})$ is the Hamiltonian for the classical coordinates $\mathbf{X}$ and momenta $\mathbf{P}$. We now treat the $\mathbf{X}$ coordinates classically and the trace operation in Eq. (3) is to be interpreted as $\mathrm{Tr} = \mathrm{Tr}_{\mathbf{X}}\mathrm{Tr}_Q$ where $\mathrm{Tr}_{\mathbf{X}} = \int d\mathbf{X}\, d\mathbf{P}$. Let $\Psi_{in}(Q,\mathbf{X})$ and $\Psi_{fn}(Q,\mathbf{X})$ represent the stationary eigenstates of $h_i(Q,\mathbf{X})$ and $h_f(Q,\mathbf{X})$ with energy eigenvalues with E_{in} and E_{fn}, respectively. Here i and f label electronic states and n and n' label the vibrational states. Clearly E_{in} and $E_{fn'}$ depend on the positions of the classical degrees of freedom, i.e.,

$$h_i(Q,\mathbf{X})\Psi_{in}(Q,\mathbf{X}) = E_{in}(\mathbf{X})\Psi_{in}(Q,\mathbf{X}), \quad (5a)$$

$$h_f(Q,\mathbf{X})\psi_{fn'}(Q,\mathbf{X}) = E_{fn'}(\mathbf{X})\psi_{fn'}(Q,\mathbf{X}). \quad (5b)$$

At low temperatures ($\beta\to\infty$) such that only the ground vibrational state ψ_{io} of h_i contributes to the trace, it is easy to show that $C(t)$ can be approximated by

$$C_o(t) = \int d\mathbf{X} \int d\mathbf{P}\, e^{-\beta H(\mathbf{P},\mathbf{X})}\langle\phi_f(t)|\phi_i(t)\rangle Z_0^{-1}, \quad (6a)$$

where

$$Z_0 = \int d\mathbf{x} \int d\mathbf{P}\, e^{-\beta H(\mathbf{P},\mathbf{X})}$$

and

$$|\phi_i(t)\rangle \equiv \mu_{if} e^{-iH_i t/\hbar}|\psi_{i0}\rangle$$

and

$$|\phi_f(t)\rangle \equiv e^{-iH_f t/\hbar}\mu_{if}|\psi_{io}\rangle. \quad (6b)$$

For simplicity we make the Condon approximation, i.e., μ is independent of Q, although this is not always justified.[15] Equations (6) can thus be evaluated by propagating $|\psi_0\rangle$ on the upper and lower surface for a time t and then evaluating the overlap. The states $|\phi_{i(f)}(t)\rangle$ obey the time dependent Schrödinger equation

$$i\hbar\frac{\partial|\phi_{i(f)}(t)\rangle}{\partial t} = \{T_Q + V_{i(f)}(Q) + V[Q,\mathbf{X}(t)]\}|\phi_{i(f)}(t)\rangle, \quad (7)$$

where the potential $V[Q,\mathbf{X}(t)]$ is a function of the classical trajectory $\mathbf{X}(t)$, and hence is time dependent. The trajectory $\mathbf{X}(t)$ is obtained by solving the classical equations of motion. It is shown in the Appendix that the time dependent potential seen by the classical coordinates $\mathbf{X}(t)$ is given by

$$W_{cl}^{i(f)} = u[\mathbf{X}(t)] + \langle\psi_{i(f)}(t)|V[Q,\mathbf{X}(t)]|\psi_{i(f)}(t)\rangle. \quad (8)$$

It is obvious that $W_{cl}^{i(f)}$ depends on the electronic state of Br_2. Equation (7) and Hamilton's equation for $\mathbf{X}(t)$, and $C(t)$ with the potential given by Eq. (8), constitute a self-consistent set of equations for the mixed quantum classical system.

For purposes of computation $|\psi_{i0}\rangle$ is taken to be a Gaussian wave packet[13]:

$$|\psi_{i0}\rangle| = \exp\left(\frac{i}{\hbar}\{A_t(Q-Q_t)^2 + [P_t(Q-Q_t) + D_t]\}\right) \quad (9)$$

and A_t, Q_t, P_t, D_t are time dependent parameters whose equations of motion are given below.[13] Following Heller, we assume that the effective time dependent potential seen by the quantum coordinate can be expanded in a Taylor series about Q_t, i.e.,

$$V_{i(f)}^{\mathrm{eff}}(Q) = V_{i(f)}^0(Q_t) + V'_{i(f)}(Q_t)(Q-Q_t) + \tfrac{1}{2}V''_{i(f)}(Q_t)(Q-Q_t)^2 + \cdots. \quad (10)$$

If the effective potential is truncated after the quadratic term and if Q_t and P_t are assumed to satisfy Newton's equation of motion A_t and D_t can be shown to obey

$$\dot{A}_t = -\frac{2}{m}A_t^2 - \frac{1}{2}V''_{i(f)}(Q_t);\quad \dot{D}_t = \frac{i\hbar}{m}A_t + P_t\dot{Q}_t - E_{i(f)}. \quad (11)$$

Given the initial values of A_0, D_0, Q_0, and P_0, the wave function at time t can be determined by integrating Eq. (11) along with the Hamilton equations for P_t and Q_t:

$$\dot{P}_t = -\partial H/\partial Q_t;\quad \dot{Q}_t = \partial H/\partial P_t \quad (12)$$

with

$$H = P_t^2/2m + V_{i(f)}(Q_t) + V[Q_t, X(t)]. \quad (13)$$

To proceed we approximate the average potential seen by the classical coordinates $\mathbf{X}$ due to the quantum coordinate Q by the potential obtained by localizing the quantum degree freedom at its classical value Q_t, i.e.,

$$\langle\psi_{i(f)}|V(Q,\mathbf{X})|\psi_{i(f)}\rangle \simeq V[Q_t,\mathbf{X}(t)]. \quad (14)$$

This is valid as long as the width of the wave packet remains much less than the range of the potential. Equations (11) and (12) determine the time evolution of the wave packet and the trajectory of the classical degrees of freedom is obtained by solving the Hamilton's equations. The potential experienced by the classical coordinates is given by substituting Eq. (14) into Eq. (8).

The potential seen by the quantum degree of freedom Q is highly anharmonic and hence the locally quadratic assumption for the effective potential is in general not adequate. This leads to an anomolously large spreading of the wave packet and consequently only short time spectra can be constructed from this formalism. To circumvent this problem the frozen Gaussian wave packet is adopted. A heuristic justification of the frozen Gaussian approximation (FGA) has been given by Heller.[16,17] Substitution of Eq. (9) into Eq. (7) gives

$$\begin{aligned} i\hbar|\psi_{i0}\rangle &= -[\dot{A}_t(Q-Q_t)^2 - 2A_t(Q-Q_t)\dot{Q}_t \\ &\quad + \dot{P}_t(Q-Q_t) - P_t\dot{Q}_t + \dot{D}_t]|\psi_{i0} \\ &= \{T_Q + V_{i(f)}(Q) + V[Q,\mathbf{X}(t)]\}|\psi_{i0}. \end{aligned} \quad (15)$$

Multiplication of Eq. (14) by ψ_{i0}^* followed by integration over Q gives

$$-\dot{A}_t\langle\psi_{i0}|(Q-Q_t)^2\psi_{i0}\rangle + P_t\dot{Q}_t = \langle E_{i(f)}(t)\rangle, \quad (16)$$

where

$$\langle E_{i(f)}(t)\rangle = \langle\psi_{i0}|\{T_Q + V_{i(f)}(Q) + V[Q,\mathbf{X}(t)]\}|\psi_{i0}\rangle. \quad (17)$$

The FGA amounts to setting $\dot{A}_t = 0$ giving

$$\dot{D}_t = P_t\dot{Q}_t - \langle E_{i(f)}(t)\rangle. \quad (18)$$

Thus the wave packet at time t can be obtained by integrating Eqs. (12) and (18) given the intitial value of the parameters D_0, P_0, and Q_0. Notice that in the FGA the action that appears in the equation of motion for D_t is different from that in the TGA [cf. Eqs. (11) and (18)].

In all the calculations described in this paper the real part of A_0 is chosen to be zero and the imaginary part of the A_0 is chosen in accordance with the frequency of the initial electronic state suitably modified by the surroundings, i.e.,

$$\mathrm{Im}\, A_0 = im\bar{\omega}/2, \tag{19}$$

where

$$\bar{\omega} = \left\{\left[\frac{\partial^2 V_{i(f)}(Q)}{\partial Q^2} + \frac{\partial^2 V(Q,\mathbf{X})}{\partial Q^2}\right]_{Q=Q_0}/m\right\}^{1/2}. \tag{20}$$

This choice of $\bar{\omega}$ includes the distortion due to the argon matrix. The parameter Q_0 is set equal to the equilibrium gas phase value Q_e, of the appropriate electronic state of Br_2. Although the Ar atoms perturb the equilibrium value Q_e, the shift was found to be negligible. This was inferred from the potential of mean force. Finally, P_0 is taken to be zero.

To implement this procedure one must solve Hamilton's equations to follow the time evolution of the classical degrees of freedom for a given $(\mathbf{X}_0, \mathbf{P}_0)$. This generates a time dependent field in which the wave packet ψ_0 moves. The state of the quantum system, ψ_0 in turn determines the potential for the classical coordinates. Solving these equations self-consistently allows determination of $|\psi_{i(f)}(t)\rangle$ and $C(t)$ and the line shape $I(\omega)$ can be obtained by performing the requisite Fourier transform.

III. CALCULATIONS

Semiclassical wave packet dynamics allows determination of the electronic absorption and emission spectra of Br_2 in an argon matrix, a system that has been studied experimentally by Bondebey *et al.*[5] The details of the preparation and the structural characterization of the matrix system will be described in a future paper.[18] In this study we consider only the A state of Br_2 for absorption and the B state for emission.[5] This precludes detailed comparison with experiment because our calculations ignore curve crossing, a potentially very important mechanism for energy relaxation.[7] The system consists of 106 Ar atoms and one Br_2 molecule enclosed in a cubic box of length 15.96 Å. Periodic boundary conditions are employed. The internal potential for Br_2 for both the X, B, and A states were obtained by fitting the RKR curves to Morse functions with parameters for the X state[19] being $D_e = 23\,100k$, $\alpha = 1.94$ Å^{-1}, and the equilibrium position $Q_e = 2.28$ Å. The parameters for the B state[20] are given by $D_e = 5454.75k$, $\alpha = 2.04$ Å^{-1}, $Q_e = 2.67$ Å, and the minimum of the B state $V(Q_e) = 22\,800k$. The A state[21] is characterized by $D_e = 2948.5k$, $Q_e = 2.69$ Å, $\alpha = 2.517$ Å^{-1}, and $V(Q_e) = 20\,006k$. The Ar–Ar and Ar–Br interactions are modeled by a (6-12) Lennard-Jones potential with $\epsilon_{\mathrm{Ar\text{-}Ar}} = 145k$, $\epsilon_{\mathrm{Ar\text{-}Br}} = 157k$, $\sigma_{\mathrm{Ar\text{-}Ar}} = 3.32$ Å, and $\sigma_{\mathrm{Ar\text{-}Br}} = 3.46$ Å. The rationale for this nonstandard choice of the Lennard-Jones parameters is given elsewhere.[22] The matrix was simulated using Monte Carlo. The details will be given in a subsequent paper.[18] The system was equlibrated at 500 K and sequentially quenched to 12 K. The resulting matrix is believed to be a glassy material.[18] The spectra reported in this paper are obtained by maintaining the system at 12 K. With this initial configuration the system is further equilibrated using molecular dynamics. The equilibrium configuration and the conjugate momenta generated by the molecular dynamics method are used as the initial configuration for the purposes of integrating the classical equations of motion. It would be desirable to average the spectra over many different initial configurations [see Eq. (6a)] instead of the small number used here. The equations of motion were integrated at the start by a fourth order Runga-Kutta method (32 time steps) with a step size Δt of 5×10^{-5} ps and then for the subsequent time evolution a fifth and sixth order Adams–Moulton algorithm with a step size Δt of 4×10^{-4} ps was used. This choice of Δt was dictated by conservation of energy and the overall normalization of the wave packet.

IV. RESULTS

A. A model potential

In order to assess the accuracy of Gaussian wave packets we first present the electronic absorption spectra from the X state of Br_2 to a model excited state potential. This model is representative of the dynamics of Br_2 in the A state. After excitation to the repulsive state, the Br atoms move rapidly apart, strike their neighboring argon atoms of the matrix, lose energy, and approach each other. The excited state potential consists of a repulsive region representing the neighborhood of the inner turning point of Br_2, a repulsive region representing the outer turning points due to the matrix atoms, and a fairly constant well region connecting the two repulsive regions. This can be qualitatively represented by the one dimensional potential

$$V_f(Q) = \begin{cases} \frac{1}{2}m\omega_l^2(Q-Q_l)^2 + V_0, & Q \leqslant Q_l, \\ V_0, & Q_l < Q < Q_r, \\ \frac{1}{2}m\omega_r^2(Q-Q_r)^2 + V_0, & Q \geqslant Q_r, \end{cases} \tag{21}$$

where Q_l was set approximately to Q_e of the X state and Q_r was adjusted to give roughly the same outer turning point as we had seen in full dynamical calculations. In particular we used $Q_e \sim 2.69$ Å, $Q_r \sim 3.98$ Å, $\omega_l = \omega_r = 254.4\,\mathrm{cm}^{-1}$, and $V_0 = 10\,000$ K. The initial width parameter in A_0 was taken to be $im\omega_l/2$ and the initial condition for the trajectory parameters were taken to be $Q_0 = Q_e$ of the X state and $P_0 = 0$. With this choice of the initial wave function the wave packet was propagated using both the thawed and frozen Gaussian approximations. The band contour of the absorption spectrum, the spectrum obtained after 1.5 period propagation using the thawed wave packet and the "analytic" spectrum are shown in Figs. 1(a)–1(c). The FC spectrum shown in Fig. 1(a) is calculated by Fourier transforming the overlap function after the initial decay. Figure 1(b) shows the expected fine structure using the thawed Gaussian, but with an unusual envelope: at about 4492 nm there is a "pinch" which distorts the envelope shown in Fig. 1(a). After this point the peak spacing is also interrupted. Another pinch is evident at about 4193 nm. These features become prominent (the pinches move, however) as the propagation time is increased.

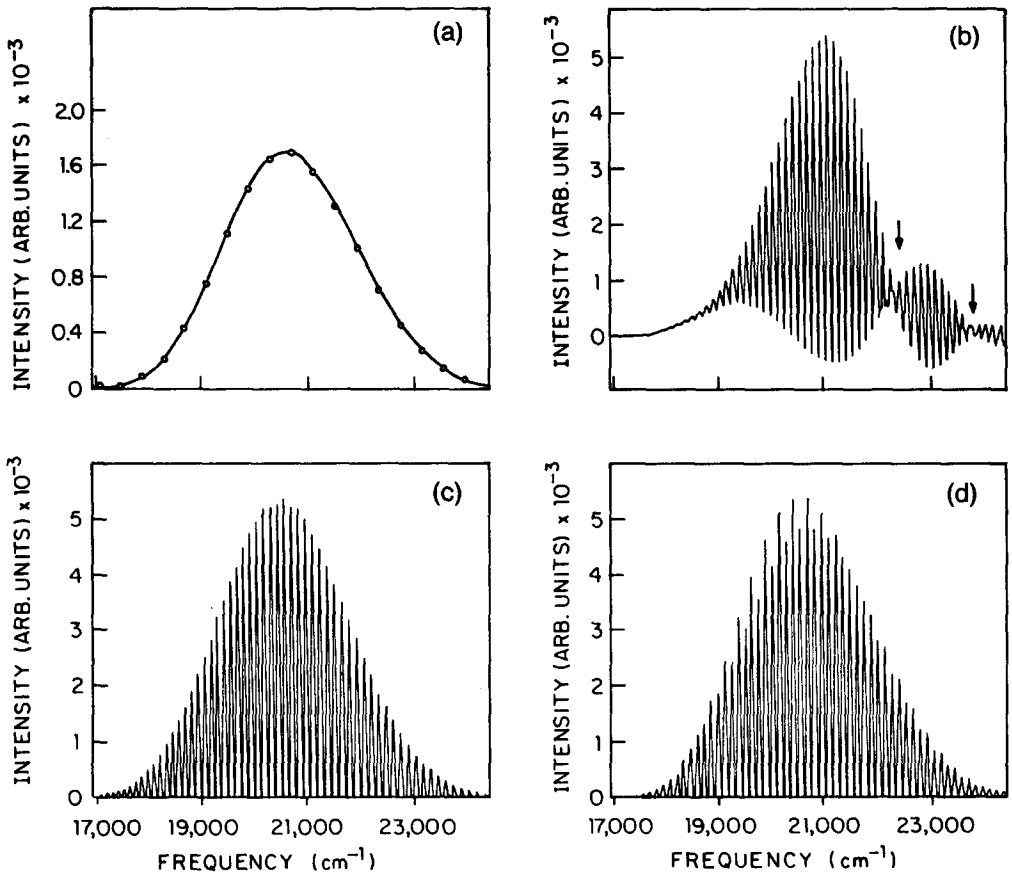

FIG. 1. These four pannels show the absorption spectra for excitation from the X state of Br_2 to a model potential as a function of frequency. The model potential is chosen to mimic the dynamics of Br_2 in the Ar matrix. The form of the potential and the relevant parameters are given in the text. The area under each curve is normalized to unity. Figures 1(a) and 1(b) show the band contour of the absorption spectra and the spectrum obtained after 1.5 periods of propagation, respectively. The spectra shown in panels (a) and (b) were obtained by propagating the wave packet using the thawed Gaussian approximation. The arrows shown in Fig. 1(b) indicate the interruption in peak spacing. In Fig. 1(c) the analytic absorption spectrum for the model potential is presented. Figure 1(d) shows the spectrum obtained using a frozen Gaussian packet after 1.5 periods of propagation.

Figure 1(c) shows that the analytic spectrum does not exhibit these anomalous features. We construct the analytic spectrum by obtaining the eigenvalues of the model potential using the WKB method and the corresponding FC factors from Fig. 1(a). The eigenvalues are given by

$$E_n = \frac{-(2m)^{1/2}Q_f + [2mQ_f^2 + (4\pi\hbar/\omega)(n+1/2)]^{1/2}}{(2\pi/\omega)}, \tag{22}$$

where $Q_f = Q_l - Q_r$ and $\omega = \omega_r = \omega_1$. Knowledge of the eigenvalues allows us to determine the FC factors accurately from the band contour [Fig. 1(a)]. As a check the resulting FC factors when summed yield 0.97. Because the "exact" spectra did not exhibit any of the pinches seen in the spectrum obtained using the thawed wave packed dynamics it seems reasonable to assume that the TGA fails for long time propagations. There are perhaps two reasons for the apparent failure of TGA dynamics: (a) the $V''(Q_t)$ for the model potential is not continuous; in particular both at Q_l and Q_r it changes discontinuously from $m\omega^2$ to 0; (b) the wave packet spreads without bound, eventually beyond the range of the potential. In Fig. 2 we show that the plot of the width of the wave packet, i.e., $[\mathrm{Im}(A_t)]^{-1/2}$ as a function of number of propagation steps. It is obvious that the width increases dramatically with time (except of course when the wave packet impinges on the repulsive walls). After about 425 steps the width becomes larger than the flat region itself. This confirms our belief that the failure of the TGA is due to the anamolous spread of the wave packet with time.

One way to bypass this problem is to adopt the FGA packet for the wave packet dynamics. The resulting spectrum obtained after 1.5 periods is displayed in Fig. 1(d). This figure shows that the intensity profile obtained using the FGA approximation is identical to the analytic spectrum. In particular the locations of the various peaks coincide with the expected transition frequencies. Given the arguments for the failure of the TGA it is not surprising that the spectrum obtained from the frozen Gaussian does not exhibit the anamolous pinches. However the intensities of the spectral lines shown in Fig. 1(d) are not in exact agreement with the analytic spectrum. Notice that in the frequency range from about 19 000 to 21 200 cm^{-1} the peak the intensities alternate. We do not understand the source of this behavior but it is probably caused by the algorithm used to numerically evaluate Fourier transformation. Nevertheless, there is a marked improvement in the spectra obtained by propagating the wave packet using the FGA.

B. Absorption spectra of Br_2 in Ar matrix

The initial width parameter of the wave packet in A_0 is given by Eq. (19) and this automatically determines D_0. Following the initial excitation to the A state repulsive wall the motion of the wave packet in the A and X states is generated for a total of 4500 time steps. The corresponding absorption spectra are plotted in Fig. 3. This figure shows that for all practical purposes the absorption spectrum in the matrix is similar to the gas phase profile. The full width at half-maximum is larger in the matrix than in the gas phase. This is rationalized by observing that the matrix appears to stabilize the potential surface of both the ground state and the excited state relative to the gas phase. Due to the attractive forces of

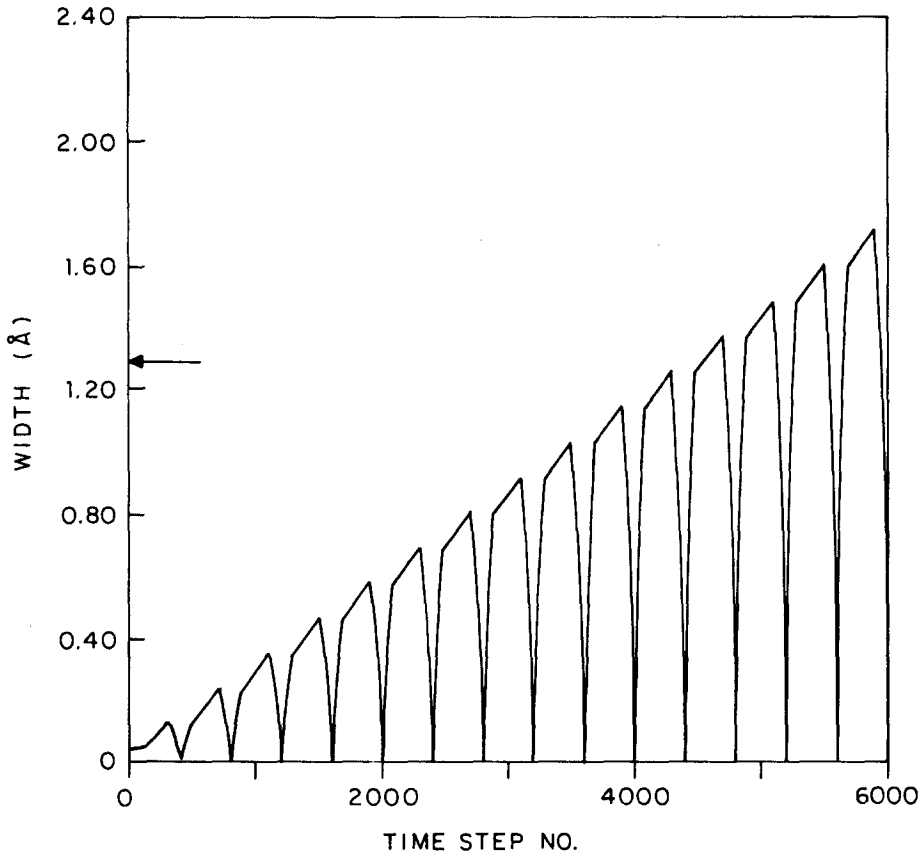

FIG. 2. Width of the wave packet in Å vs the number of time steps for Br_2 in the model potential. The arrow on the width axis indicates the extent of the flat region.

the matrix the center of the wave packet has a large velocity, and the initial overlap dies off faster in the matrix than in the gas phase leading to a slightly larger width. After the initial decay the overlap does not recur for a long time so that the absorption profile is determined by the initial decay. Similarity between the gas phase absorption spectrum and the matrix spectrum suggests that there is no "spectroscopic" cage effect, i.e., the matrix does not induce any additional quantized bound vibrational states in the gas phase continuum. This has been seen in several experimental studies of diatoms in matrices.[1,2]

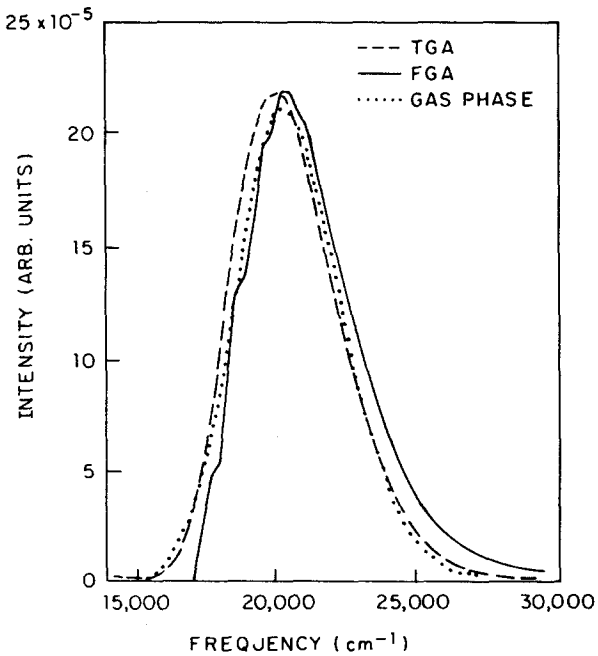

FIG. 3. The electronic absorption spectra from the $A \leftarrow X$ state of Br_2 in an Ar matrix is plotted as a function of frequency. The area under each curve is normalized to unity. The dashed line (---) is the result using the frozen Gaussian and the solid line (—) corresponds to the thawed Gaussian. For comparison, in dotted line (· · ·) the spectra in the gas phase is shown.

The advantage of molecular dynamics simulation is that one can follow the detailed classical dynamics of Br_2 in the matrix. This in turn sheds light on the relaxation mechanism after Br_2 is excited to the A state. The energy records of Br_2 and Ar matrix atoms as a function of time are shown in Figs. 4(a)–4(d). Figure 4(a) shows the potential energy V of Br_2 and in Fig. 4(b) the kinetic energy is plotted. From these figures we see that after 250 time steps the Br_2 molecule seems to have given up its excess energy and executes periodic motion in the bound part of the A state potential. Thus, although the Br_2 molecule is initially excited to 4520 cm^{-1} above the A state dissociation energy we find that the matrix atoms prevent it from permanently dissociating. Our simulation, therefore, confirms the experimental findings that in all studies involving diatoms in matrices the quantum yield to permanent dissociation is less than 10^{-4}.

Before we account for the effect of the matrix on the dynamics of Br_2 it is important to distinguish between static and dynamic perturbations due to the cage atoms. If the perturbation due to the lattice is static then this will merely induce frequency shifts but Br_2 in a static field will not make a radiationless transition. Dynamic perturbations of Br_2 can, however, induce radiationless transitions with the excess energy taken up by matrix. We refer to this as the dynamic cage

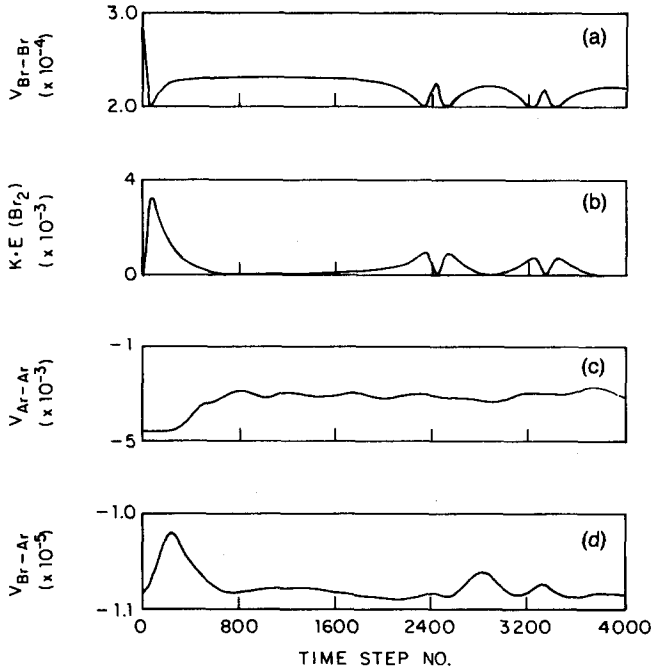

FIG. 4. Plot of energy of various subsystems in keluim as a function of the number of time steps. This is obtained by following the classical dynamics of Br_2 in an Ar matrix after excitation to the A state. Figures 4(a) and 4(b) show the internal potential energy and the kinetic energy of Br_2, respectively. Also shown in Fig. 4(b) is the kinetic energy of the matrix which remains nearly constant. Figures 4(c) and 4(d) show the potential energy of the matrix and the energy of interaction between Br_2 and Ar matrix, respectively. Each time step is equal to 4×10^{-4} ps.

effect. The absence of structure in the electronic spectrum and the formation of the dynamic cage which prevents Br_2 from dissociating can be explained in terms of efficient energy transfer from Br_2 to the cage atoms. In fact the dynamic cage effect is best illustrated in terms of the classical dynamics of Br_2 molecule in the matrix which we show in Figs. 4(a) and 4(d). After the initial excitation of Br_2, 0.58 eV above the dissociation barrier of the A state, it is seen to execute unhindered vibrational motion until it encounters the nearest cage atom. This is seen in Figs. 4(a) and 4(b) which show that the internal potential energy starts to decrease [see Fig. 4(a)] while the kinetic energy of Br_2 increases [cf. Fig. 4(b)]. At this point the Br atom suffers a violent collision with its neighboring Ar atom and transfers most of its kinetic energy to the lattice. After the collision (which occurs within the first 80 time steps), the Br atom continues to move in the same direction with reduced velocity until it reaches the outer turning point, which is approximately at 4.23 Å. Even after the first collision the Br_2 molecule is slightly above the dissociation barrier. However after it suffers a second collision [see Fig. 4(a)] Br_2 loses its excess energy and it relaxes to an intramolecular bound part of the excited potential. Notice that Fig. 4(b), which shows the plot of the kinetic energy of the Br_2, mirrors exactly the potential energy. After Br_2 relaxes to the bound part of the A state it simply undergoes periodic motion in the well. Thus Br_2 loses its excess kinetic energy in about 0.03 ps and this is the time scale of the dynamic cage effect. Because of this fast energy relaxation the inner turning point is so far to the right of the center of the original wave packet, that there is no recurrence. Therefore, the electronic absorption spectra is determined from the initial decay of the overlap leading to a spectra resembling to gas phase profile.

Now we examine the fate of the lattice after the nearest neighbor cage atom suffers the first collision. The potential energy of the matrix plotted in Fig. 4(c) shows that in about 80 time steps (or shortly after the first collision) the lattice has gained about 4000 K (0.34 eV) energy. After this initial gain in energy the potential energy of the lattice remains more or less constant. When the classical trajectory of the system is integrated for about 5600 time steps we see that the lattice seems to be at a slightly elevated temperature. Motion of the Ar atoms is extremely slow and hence the relaxation of the lattice is slow. Finally consider the Br–Ar potential energy V_{Br-Ar}, shown in Fig. 4(d). The V_{Br-Ar} energy is seen to increase with time even after the Br atom has suffered its first collision with the cage atom. This is because Br continues to travel in the same direction after collision and hence interacts very strongly with the colliding Ar atom. However after the Br_2 molecule relaxes to the bound part of the A state potential V_{Br-Ar} is seen to remain fairly constant and equal to its value at time $t = 0$. Thus almost all of the energy lost by Br_2 has been transferred to the lattice. Another interesting aspect of this simulation is that although Br_2 carriers energy of about 0.58 eV above the dissociation we have indirect evidence for the absence of transient local melting that is for the preservation of the cage.

C. Emission spectra

In order to calculate the emission spectra we equilibriate the system with Br_2 in the excited state. This equilibriation is actually achieved during the calculation of the absorption to the B state. For purposes of the simulation we study the emission from the $B\,^3\pi(0_u^+)$ state and thus we can compare our results with the experimental work of Bondebey *et al.* A Gaussian wave packet, with the parameter Im A_0 given by Eq. (20) is assumed to represent the $v' = 0$ of the B state. Following the Frank–Condon transition to the ground state the time development of the wave packet if followed both in the B state as well as in the X state. The quantity $C_0(t)$ is calculated using the $\beta\to\infty$ limit of

$$C(t) = \mathrm{Tr}\{e^{-\beta H_f}\mu_{if}e^{iH_f t/\hbar}\mu_{if}e^{-H_i t/\hbar}\}/\mathrm{Tr}\{e^{-\beta H_f}\} \quad (23)$$

in the Condon approximation; at finite temperature this would entail propogation in both the Euclidean time as well as in the Minkowski time. The wave packet is propagated in both the X and B electronic states for a total of 485 time steps and the emission spectrum thus obtained is displayed in Fig. 5(a). The striking feature is the progression in the v'' quantum number in the high frequency region of the spectrum and the absence of structure in the low frequency end. As the wave packet propagates in the X state the parameters change according to the local region of the X state. In order to resolve the spectral lines in the low frequency region we require the wave packet after one period to overlap with the initially prepared packet. Furthermore the corresponding FC factors should be appreciable. Because the packet loses energy to the lattice the FC factors for transitions to high v'' quantum numbers are negligible. As the packet develops in

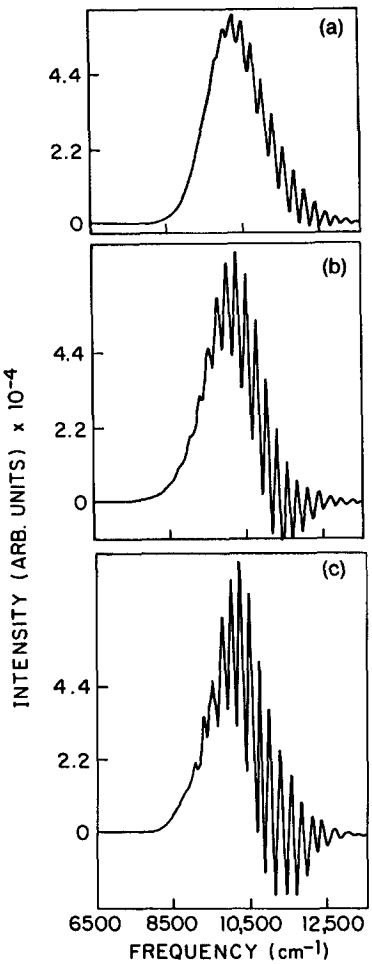

FIG. 5. Emission spectra from $X \leftarrow B$ state of Br_2 in Ar matrix as a function of frequency. The area under each pannel is normalized to unity. Figures 5(a) and 5(b) show the spectra obtained after 485 time steps using the thawed Gaussian and the frozen Gaussian, respectively. In Fig. 5(c) the spectra obtained after 1200 time steps using the frozen Gaussian is shown. Each time step is equal to 4×10^{-4} ps.

time it explores the potential region corresponding to the lower v'' quantum numbers only. Consequently, we do not observe vibrational progression in the low frequency region. This leads us to conclude that the ansatz of a single coherent state representing the $v' = 0$ state of the B state is perhaps not adequate.

In Fig. 5(b) we show the emission spectra obtained by propagating the wave packet for 485 time steps in the FGA. Like the spectrum obtained using the TGA for propagation we see a vibrational progression in v'' but unlike the spectrum shown in Fig. 2(a) we see a few well resolved lines in the low frequency region as well. This can be understood very simply by noting that in the FGA approximation the width of the wave packet which is chosen in accordance with the frequency of the upper state is kept fixed throughout the propagation. After the Frank–Condon transition the wave packet explores the potential corresponding to the X state. We noted earlier after the first recurrence the wave packet essentially explores the regions of the potential corresponding to low v'' quantum numbers only. However because the width of the wave packet which is kept fixed throughout the propagation, is larger than what it would have been had it followed the local curvature of the X state, the tail of the wave packet feels the region corresponding to high v'' quantum numbers even after the first period. The revisitation to the anharmonic region of the X state gives rise to stronger overlap with the initial wave packet compared to the TGA and this is necessary to resolve the low frequency transitions. It seems logical that one can propagate the wave packet using the FGA for longer times than seems possible by the TGA scheme. Accordingly we obtained the emission spectra after following the frozen Gaussian wave packet for 1200 steps. The resulting emission spectra which exhibits all the features shown in Fig. 5(b) is displayed in Fig. 5(c). Figure 5(c) shows that some of the peaks in the low frequency end are slightly better resolved. However one starts to notice unnatural splittings in the low frequency peaks indicative of the instability of the single Gaussian wave packet dynamics for long propagation. It should be pointed out that the emission spectra obtained after 1200 time steps by propagating the thawed Gaussian yields unphysical lines with each peak split into smaller peaks. This suggests that longer time information may be obtainable by the frozen Gaussian method than the thawed Gaussian scheme.

For purposes of comparing the effect of the matrix on the potential surface of the ground state and on the spacing T_e we make a spectral analysis. This is made using the spectra obtained by the TGA. Assuming that the highest peak corresponds to $B\,(V' = 0) \rightarrow X\,(V'' = 11)$ (which would be in accord with the experimental assignment of Bondebey *et al.*[5]) the ω_e and $\omega_e X_e$ can be computed from the vibrational progression, turn out to be 315 and 1.55 cm^{-1}, respectively, and are in excellent agreement with the gas phase values $\omega_e^g = 321$ cm^{-1} and $(\omega_e X_e)^g = 1.61$ cm^{-1}. The value of T_e turns out to be 13 770 cm^{-1} and this is 1645 cm^{-1} lower than the experimental value. Bondebey *et al.*[5] infer that the matrix stabilizes the electronic states of Br_2 by about 476.3 cm^{-1} and this shift to lower energies is typical of most matrix isolated compounds. The discrepancy of 1169 between the experimental value and our simulation result may be indicative of the incorrect parameters characterizing the Br–Ar potentials. If the interaction of the Ar atom with the Br when Br_2 is in the B state is adequately given by the LJ potential then the simulation can be systematically used to estimate the LJ parameters. This study suggests that Br–Ar interaction depends strongly on the electronic state of Br_2. The desired blue shift of 1169 cm^{-1} can be obtained by adjusting both the ϵ and σ values. Thus the $\epsilon_{\text{Ar-Br}(B)}$ has to be less than $\epsilon_{\text{Ar-Br}(X)}$ and the $\sigma_{\text{Ar-Br}(X)}$ has to be made less than $\sigma_{\text{Ar-Br}(B)}$ to achieve the desired blue shift. One can quite easily do a two parameter search to map out the sensitivity of the matrix shift to the changes in the Br–Ar interactions. (Based on a very simple calculation we recommend that $\epsilon_{\text{Ar-Br}} = 127.4$ K and $\sigma_{\text{Ar-Br}} = 3.54$ Å be used when Br is in the B state.)

V. CONCLUSIONS

In this article we have reported the results of a simulation of electronic absorption and emission spectra of Br_2 in an Ar matrix. The appropriate correlation functions were evaluated semiclassically using the coherent state representation. This amounts to propagating the Gaussian wave packet in time and this was achieved by the methods pioneered by Heller over the last several years.[11,12,16] Based on this study we make the following recommendations:

(a) The single Gaussian wave packet method (SGW), although intuitively very appealing, is most suited for ob-

taining short time information in many-body systems with small anharmonicities. The assumption of a locally quadratic potential breaks down when the wave packet explores anharmonic regions of the potential. This leads to an unphysical spreading of the Gaussian wave packet.[25–28] Unfortunately, in the calculation of electronic spectra in matrices the potential experienced by the quantum system is highly anharmonic. Therefore it appears that the wave packet method in the thawed Gaussian approximation (and to a lesser extent the FGA) is not suitable for calculating high resolution spectra. We have shown that there is marked improvement in the quality of spectra when the frozen Gaussian scheme was used. But even the FGA is not trustworthy when high resolution emission spectra is desired.

(b) One of the ways of improving the quality of the wave function is to determine the wave packet parameters variationally. In this method we calculated the parameters A_t, Q_t, P_t, and D_t using the time dependent variational principle.[29,30] Since we do not make locally quadratic approximation for the potential it is expected that the variational method would yield a "better" wave function than the TGA or the FGA. The only approximation made is the ansatz that a single Gaussian wave packet adequately describes the state of the quantum coordinate. We used the variational wave packet method to calculate the gas phase emission spectrum from the $B \leftarrow X$ state. The time dependent equations for the parameters of the wave packet were integrated using the fourth order Runga-Kutta algorithm with a time step of 10^{-4} ps. The wave packet did not spread more than 0.3 Å (the range of the potential being 0.49 Å) over the entire time of propagations of about 1.6 ps. This is to be constrasted with the TGA for the propagation which resulted in wave packet spreading to 0.5 Å in about 0.8 ps. However, the resulting emission spectra obtained from the variational wave function after propagating for 0.8 ps was found to possess spurious features. Since the only approximation made in this calculation is in the choice of the state of the quantum coordinate it is clear that the single Gaussian is an inadequate approximation to the true ground state wave functions. However it may be possible to choose a linear combination of Gaussian wave packets[31,32] and determine the coefficients using the variation principle. Lee and Heller[32] have used this method to calculate the gas phase photodissociation spectrum of CH_3I. In principle, this is an obvious extension but this definitely makes the wave packet dynamics more cumbersome and one loses the remarkable simplicity of the single Gaussian wave packet method. Furthermore this may not be very practical when one is dealing with finite temperature many body systems.

(c) Despite the shortcomings of the SGW method for the problem considered in this paper we have shown that it is possible to glean some of the qualitative aspects of matrix isolated spectra commonly found in experiments. In particular the results obtained for absorption confirm the analysis of Bondebey and Brus.[1,2] The low resolution emission spectrum shows the vibrational progression seen in the experiments. Furthermore, assuming that Br and Ar interact via a 6-12 Lennard-Jones potential, the emission spectrum can be used to obtain the Br–Ar potential when Br is in the excited state.

(d) In light of the difficulties with the Gaussian wave packet dynamics it seems necessary to look for alternate methods. One possiblity is to use the coherent state path integral method introduced by Klauder.[33–36] In this formulation the propagator $e^{-\beta H}$ (or e^{iHt}) is expressed in the coherent state representation and consequently the measure involves both the coordinates as well as momenta. Each step of the propagation can be done either semiclassically or by using Monte Carlo techniques. The use of coherent state path integrals for problems of chemical interest has also been hinted at by the Heller[37] but so far they have not been tested on any system. Other methods have been proposed for calculating medium effects on spectra.[38–41]

(e) Recently we have shown[42] that path integral methods can be used to obtain absorption and emission spectra by directly obtaining the relevant real time information. This is not restricted to any form for the potential and more importantly one does not have to invoke the Condon approximation either. It is hoped that this theory may provide a viable alternative to obtaining spectroscopic information in the condensed state.

APPENDIX

In this Appendix we comment on the use of Eq. (8) which gives the potential seen by the classical coordinates X when it is interacting with the quantum coordinate. The justification for this is contained in the work of Pechukas.[43] The Hamiltonian for the mixed-quantum classical system can be written as

$$H(\mathbf{P}, \mathbf{X}, P_Q, Q) = H(\mathbf{P}, \mathbf{X}) + H(P_Q, Q) + V(Q, \mathbf{X}) = H(\mathbf{P}, \mathbf{X}) + h(Q, \mathbf{X}). \quad \text{(A1)}$$

The propagator for transition from $(\mathbf{X}_i, Q_i)$ at time t to $(\mathbf{X}_f, Q_f)$ at time $t + \epsilon$ is given by the Feynman path integral formula as

$$K(\mathbf{X}_f, Q_f, t+\epsilon, \mathbf{X}_i, Q_i, t) = \int D[Q]\, D[\mathbf{X}] \exp\left\{\frac{i}{\hbar}\int_t^{t+\epsilon} L\, dt\right\}, \quad \text{(A2)}$$

where L is the appropriate Lagrangian for the mixed-quantum classical system. As emphasized by Pechukas in order to obtain the "classical" path $\mathbf{X}(t)$ while the quantum system evolves from $\psi(Q, t)$ to $\psi(Q, t+\epsilon)$ one needs only the reduced propagator $K_r(\mathbf{X}_f, t+\epsilon, \mathbf{X}_i, t)$ and this is given by

$$K(\mathbf{X}_f, t+\epsilon, \mathbf{X}_i, t) = \int D[X] \exp\left\{\frac{i}{\hbar} S_1\right\} T[\mathbf{X}], \quad \text{(A3)}$$

where

$$S_1 = \int_t^{t+\epsilon} L(\dot{\mathbf{X}}, \mathbf{X}) dt \quad \text{(A4)}$$

and

$$L(\dot{\mathbf{X}}\mathbf{X}) = \int_{i=1}^{f} \tfrac{1}{2} m_i \dot{\mathbf{X}}_i^2 - V(\mathbf{X}). \quad \text{(A5)}$$

The transition probability $T[\mathbf{X}]$ is given by

$$T[\mathbf{X}] = \int dQ \psi^*(Q, t)\psi(Q, t+\epsilon)$$
$$= \int dQ\, \psi^*(Q, t) e^{-i\epsilon h/\hbar}\psi(Q, t). \quad \text{(A6)}$$

Remember that $\psi(Q, t)$ satisfies that time dependent Schrödinger equation.

To obtain the classical path $\mathbf{X}(t)$ we make the stationary phase approximation to Eq. (A3) giving rise to the following condition:

$$\delta\{S_l[\mathbf{X}(t)] + \hbar \operatorname{Im} \ln T[\mathbf{X}]\} = 0. \quad \text{(A7)}$$

This is the "least action principle" for $\mathbf{X}(t)$ when it interacts with the quantum subsystem. The "solution" to Eq. (A6), if it exists at all, is expected to be very complicated and the resulting interaction can be highly nonlocal, etc. To make progress we assume that ϵ is small and hence we use a perturbation approach to obtain a computationally useful formula for the effective potential seen by the classical coordinates. From the first order perturbation theory we get

$$\delta T[\mathbf{X}] = -i/\hbar\epsilon\langle\psi(Q, t)|h\,|\psi(q, t)\rangle \quad \text{(A8)}$$

using Eqs. (A8) and (A7) the classical path is seen to satisfy the equation

$$M\ddot{\mathbf{X}} = -\frac{\partial \mathbf{H}}{\partial \mathbf{X}}(\mathbf{P}, \mathbf{X}) - \frac{\partial}{\partial \mathbf{X}} V_{\text{eff}}(\mathbf{X}, t), \quad \text{(A9)}$$

where

$$V_{\text{eff}}(\mathbf{X}, t) = \langle\psi(Q, t)|h(Q, \mathbf{X})|\psi(Q, t)\rangle. \quad \text{(A10)}$$

In obtaining Eq. (A8) we have assumed that ϵ is very small. This can always be arranged in any simulation and is in the spirit of the semiclassical solution to the TDSE advocated here. As a final note we add that the above approximation leads to conservation of energy, i.e.,

$$\frac{d}{dt}\langle\psi(t)|H(\mathbf{P}, \mathbf{X}, P_Q, Q)|\psi(t)\rangle \equiv 0. \quad \text{(A11)}$$

Thus this allows us to calculate energy exchange between the quantum subsystem and the classical system and if $\psi(t)$ can be obtained accurately one should be able to study the relaxation of the quantum system as well as observe any elementary excitation associated with the medium.

[1] V. E. Bondybey and L. E. Brus, Adv. Chem. Phys. **41**, 269 (1980).
[2] V. E. Bondybey and L. E. Brus, in *Radiationless Transitions*, edited by S. H. Lin (Academic, New York, 1980).
[3] D. J. Diestler, Adv. Chem. Phys. **42**, 305 (1980).
[4] B. S. Ault, W. F. Howard, and L. Andrews, J. Mol. Spectrosc. **55**, 217 (1975).
[5] V. E. Bondybey, S. S. Bearder, and C. Fletcher, J. Chem. Phys. **64**, 5243 (1976).
[6] M. Mandich, P. Beeken, and G. W. Flynn, J. Chem. Phys. **77**, 702 (1982).
[7] P. Beeken, E. A. Hanson, and G. W. Flynn, J. Chem. Phys. **78**, 5892 (1983).
[8] G. W. Robinson and R. P. Frosch, J. Chem. Phys. **37**, 1962 (1962); **38**, 1187 (1963); K. F. Freed, Acc. Chem. Rev. **11**, 74 (1978).
[9] M. F. Herman and B. J. Berne, Chem. Phys. Lett. **77**, 163 (1981).
[10] M. F. Herman and B. J. Berne, J. Chem. Phys. **76**, 4103 (1983).
[11] E. J. Heller, J. Chem. Phys. **62**, 1544 (1975).
[12] E. J. Heller, Acc. Chem. Res. **14**, 268 (1981).
[13] For an application to many-body system see N. Korbin and K. Singer, Mol. Phys. **46**, 671 (1982).
[14] M. Lax, J. Chem. Phys. **20**, 1752 (1952).
[15] For an example see J. Tellinghuisen, J. Chem. Phys. **76**, 4736 (1982).
[16] E. J. Heller, J. Chem. Phys. **75**, 2923 (1981).
[17] A more formal justification has been proposed by M. F. Herman and E. Kluk, Chem. Phys. **91**, 27 (1984).
[18] D. Thirumalai and B. J. Berne (in preparation).
[19] D. McQuarrie *Statistical Mechanics* (Harper and Row, New York, 1976).
[20] R. F. Barrow, T. C. Clark, J. A. Coxon, and K. K. Yee, J. Mol. Spectrosc. **51**, 428 (1974).
[21] J. A. Coxon, J. Mol. Spectrosc. **41**, 548 (1972).
[22] E. J. Bruskin, Ph.D thesis, Columbia University (unpublished).
[23] V. E. Bondebey and L. E. Brus, J. Chem. Phys. **62**, 620 (1975).
[24] V. E. Bondebey and L. E. Brus, J. Chem. Phys. **64**, 3724 (1976).
[25] J. Brickmann and P. Russegger, J. Chem. Phys. **75**, 5744 (1981).
[26] J. Brickmann and P. Russegger, Chem. Phys. (in press).
[27] J. Brickmann, J. Chem. Phys. **78**, 1884 (1983).
[28] M. M. Nieto and L. M. Simmons Jr., Phys. Rev. Lett. **41**, 207 (1978).
[29] E. J. Heller, J. Chem. Phys. **64**, 63 (1976).
[30] A. D. McLachlan, Mol. Phys. **8**, 39 (1964).
[31] R. D. Coalson and M. Karplus, Chem. Phys. Lett. **90**, 301 (1982); J. Chem. Phys. **79**, 6150 (1983).
[32] S. Y. Lee and E. J. Heller, J. Chem. Phys. **76**, 3035 (1982).
[33] J. C. Klauder, Ann. Phys. **11**, 123 (1960).
[34] C. Garrod, Rev. Mod. Phys. **38**, 483 (1966).
[35] H. Kuratsuyi and Y. MiZobuski, Phys. Lett. A **82**, 279 (1981).
[36] Y. MiZobuski, Prog. Theor. Phys. **65**, 1450 (1981).
[37] E. J. Heller, Chem. Phys. Lett. **34**, 321 (1975); (private communication).
[38] S. Mukamel, Phys. Rep. **93**, 1 (1982).
[39] S. Mukamel, J. Chem. Phys. **77**, 173 (1982).
[40] R. Islampour and S. Mukamel, Chem. Phys. Lett. **107**, 239 (1984).
[41] R. Islampour and S. Mukamel, J. Chem. Phys. **80**, 5487 (1984).
[42] D. Thirumalai and B. J. Berne, Chem. Phys. Lett. (in press).
[43] P. Pechukas, Phys. Rev. **181**, 174 (1969).